HHS Public Access

Author manuscript

Pediatr Radiol. Author manuscript; available in PMC 2023 February 01.

Published in final edited form as:

Pediatr Radiol. 2022 February ; 52(2): 228–248. doi:10.1007/s00247-021-05264-9.

Quantitative Renal MRI: MR Urography

J. Damien Grattan-Smith[1], **Jeanne Chow**[2], **Sila Kurugol**[2], **Richard A Jones**[1]

[1)]Department of Radiology, Children's Healthcare of Atlanta, Atlanta, Georgia, USA.

[2)]Department of Radiology, Boston Children's Hospital, Boston, Massachusetts, USA

Abstract

The goal of functional renal imaging is to identify and quantitate irreversible renal damage and nephron loss, as well as potentially reversible hemodynamic changes. MR urography has evolved into a comprehensive evaluation of the urinary tract that combines anatomical imaging with functional evaluation in a single test without ionizing radiation. Quantitative functional MR imaging is based on dynamic contrast-enhanced MR acquisitions that provide progressive, visible enhancement of the renal parenchyma and urinary tract. The signal changes related to perfusion, concentration and excretion of the contrast agent can be evaluated using both quantitative and qualitative measures. Functional evaluation with MR has continued to improve as a result of significant technical advances allowing for faster image acquisition as well as the development of new tracer kinetic models of renal function. The most common indications for MR urography in children are the evaluation of congenital anomalies of the kidney and urinary tract including hydronephrosis and renal malformations, and the identification of ectopic ureters in children with incontinence. In this paper, we review the underlying acquisition schemes and techniques used to generate quantitative functional parameters including the differential renal function (DRF), asymmetry index, mean transit time (MTT), signal intensity versus time curves as well as the calculation of individual kidney glomerular filtration rate (GFR). Visual inspection and semi-quantitative assessment using the renal transit time (RTT) and calyceal transit times (CTT) are fundamental to accurate diagnosis and are used as a basis for the interpretation of the quantitative data. The importance of visual assessment of the images cannot be overstated when analyzing the quantitative measures of renal function.

Introduction

In pediatric imaging, quantitative tests of renal function are used to identify the presence of renal disease, determine its progression, decide when surgery is needed and monitor the response to treatment. Traditional imaging assessment of the kidneys is based on measuring renal mass or renal uptake and excretion as surrogate markers of renal function.

Over the last two decades, MR urography has evolved into a comprehensive evaluation of the urinary tract that combines anatomical imaging with functional evaluation in a single test without ionizing radiation [1,2,3,4,5,6,7,8]. Functional MR imaging is based on dynamic contrast-enhanced MR acquisitions that provide progressive, visible enhancement of renal

Corresponding Author: Damien Grattan Smith, MD, 3944 Club Drive, Atlanta, Ga 30319, Damien.grattansmith@me.com.

parenchyma and urinary tract. The signal changes related to perfusion, concentration and excretion of the contrast agent can be evaluated using both quantitative and qualitative measures. Several authors have shown that MR urography provides comprehensive evaluation of urinary tract abnormalities similar to, or better than, renal scintigraphy [1, 9,10,11,12,13,14,15]. The interpretation of MR urography is based on the principles established by intravenous urography but takes advantage of its greater intrinsic spatial, contrast and temporal resolution [16,17,18].

The initial functional applications of MR urography mimicked diuretic renal scintigraphy in assessing renal drainage by calculating renal transit times, measuring relative renal function of the kidneys and generating signal intensity and time curves [19,20,21]. Functional evaluation with MR has continued to improve as a result of significant technical advances allowing for faster image acquisition as well as the development of new tracer kinetic models of renal function [1,2,3,4,5,6,7,8]. Recent technical advances have shown quantitative MR to be both feasible and reliable for calculating the glomerular filtration rate (GFR) in children [22]. Several groups have described different approaches to MR urography with variations both in the imaging protocols as well as methods used to perform functional analysis [23,24,25,26,27]. Variations in imaging technique differ in the approach to sedation, timing of furosemide administration, as well as the administration and dose of contrast agent. While no consensus protocol has been established, we currently prefer three-dimensional (3-D) techniques, especially with the development of compressed sense reconstructions and parallel imaging with high acceleration factors. Golden angle radial sparse parallel MRI (GRASP-MRI) is a particularly attractive option because of its motion insensitivity.

The most common indication for MR urography in children is the evaluation of congenital anomalies of the kidney and urinary tract including hydronephrosis, renal malformations, and identification of ectopic ureters in children with incontinence. Accurate functional evaluation in these children is essential to guide their management.

In this paper we review the underlying acquisition schemes and techniques used to generate quantitative functional parameters including the differential renal function (DRF), asymmetry index, mean transit time (MTT), signal intensity versus time curves as well as the calculation of individual kidney GFR. Visual inspection and semi-quantitative assessment using the renal transit time (RTT) and calyceal transit times (CTT) are fundamental to accurate diagnosis and are used as a basis for the interpretation of the quantitative data. With MR urography, the functional analysis must be correlated with the anatomical appearance to provide comprehensive assessment of the urinary tract pathophysiology.

Overview of renal function

The functions of the kidney are complex and include: (1) excretion of surplus water and the final metabolic products; (2) maintenance of the constant composition of body fluids; (3) preservation of the acid–base balance; and (4) endocrine function manifested as production and release of erythropoietin, renin and 1,25 dihydroxycholecalciferol. The mechanisms of

renal function are glomerular filtration, tubular reabsorption and tubular secretion, which produces the excreted urine. Renal function is determined by both the number and the quality of nephrons. Currently, GFR estimates are the best overall indices of the level of renal function because assessing tubular function is more complicated than assessing GFR. Traditionally it has been assumed that renal tubular function declined in parallel with glomerular filtration, but this assumption has been challenged in people with moderate or severe chronic kidney disease [28]. It should also be noted that the majority of frequently used clinical tests for assessing GFR (such as serum creatinine and cystatin C, and nuclear medicine tests such as Tc-99 m DTPA [technetium-99 m-diethylene-triamine-pentaacetate]) reflect the global (combined) renal function of both kidneys rather than single kidney function.

Glomerular filtration rate is the product of nephron number and single-nephron GFR. Following nephron loss, compensatory changes in surviving nephrons are commonly observed in clinical practice [29]. This leads to less striking loss of total renal function than anticipated by the extent of anatomical damage. In fact, the earliest nephron losses are likely to be invisible because of functional compensation, which keeps the GFR in the normal range. This presumably explains why most people have normal renal function in the presence of unilateral renal disease. Any deficit in the number of nephrons at birth or a subsequent loss of nephrons is permanent. If there is a loss of nephrons, hemodynamic changes increase the single-nephron GFR to preserve renal function in the short term, but long-term this is a maladaptive response because it preserves whole-kidney GFR at the expense of progressive nephron injury [30].

Nephrogenesis begins in the fetus and is completed in humans by term, and no new nephrons are formed after birth [29]. Neonatal kidneys are structurally and functionally immature. After birth there is continued structural and functional maturation of the kidneys. The kidney glomeruli occupy a much larger cortical volume during the first 2 months after birth (18%) in comparison with adults (8.5%) [31]. The GFR increases rapidly during the first 3 months after birth and then increases more slowly until the adult level is reached at the end of the 2nd year. The kidney reaches its full anatomical and functional maturity by the end of the third decade of life. Most maturational (as well as compensatory) renal growth is primarily dependent on proximal tubular growth [32]. The proximal tubular mass constitutes more than 50% of the volume of the normal kidney, and growth of the proximal tubule accounts for the increasing size of the kidney from late gestation through early childhood. Proximal tubule length increases from 2 mm at birth to 12 mm in the adult and its rate of growth outstrips that of the glomerulus [33].

The number of nephrons per kidney is highly variable and averages about 900,000, with a range from 210,000 to 2.7 million nephrons [34]. Current methods for calculating nephron number in living humans require a kidney biopsy and calculation of cortical volume [34]. Like many human organs, the kidneys have innate mechanisms to adapt to increased “work demand” or stress. The kidney has a functional reserve capacity both at the glomerular and tubular levels [35,36,37]. In normal people, baseline GFR changes throughout the day depending on the physiological requirements. GFR can also increase in response to stimuli such as acute oral protein load or intravenous amino acid infusion. Nephron

number and single-nephron GFR are fundamental properties of the kidney that if measured independently might help distinguish irreversible nephron loss from reversible changes in renal hemodynamics.

Evaluation of renal tubular function is challenging and has received little attention from an imaging standpoint. The renal tubule is tasked with an enormous portfolio of responsibilities, most notably the handling of electrolytes, water and amino acids, catabolism of various proteins and the active secretion of endogenous and exogenous acids. The tubular flow rate of urine depends in large part on the GFR, which is regulated by the tubuloglomerular feedback and the myogenic mechanism [38]. The tubuloglomerular feedback system is a key regulator of GFR and the delivery of water and electrolytes to the distal nephron. A higher blood pressure in the glomerulus increases single-nephron GFR and raises the rate of fluid flow throughout the tubule. In normal kidneys, approximately 99% of the glomerular utrafiltrate is reabsorbed in the tubules. In a healthy individual the two components of the nephron — glomerular and tubular — work in concert. However, when the kidney is diseased or injured, the glomerular and tubular function might be affected equally, or their form and functional capacity might diverge. Recently attention has shifted to injury to the glomerular–tubular junction and the formation of atubular glomeruli [33].

Historically, kidney size or volume has been used as the most simple indicator of renal disease, particularly chronic renal disease. The volume of the kidney has been used as a surrogate of functioning renal mass and nephron endowment [39]. Previous studies have shown a strong correlation between the total renal volume (i.e. sum of the volume of both kidneys) and the GFR [40, 41]. Decrease in renal size and volume is considered a sign of irreversible renal disease because most kidneys shrink with disease progression and loss of GFR [35, 40]. Small kidneys, whether hypoplastic or scarred, have a decreased number of nephrons. Large kidneys have either considerable nephron endowment or have hypertrophy of the nephrons, as is seen with compensatory hypertrophy in children with single kidneys. Although kidney volume has been used as a surrogate measure of nephron number, its validity in adults has been questioned because of the compensatory ability of the nephrons [42].

Magnetic resonance measurement of renal function

The steps required for an accurate measurement of GFR using MR are outlined next, including:

1. patient preparation,
2. use of a suitable dynamic contrast-enhanced sequence,
3. motion correction and segmentation of the kidney(s),
4. conversion of the MR signal to concentration of the contrast agent and
5. selection of an appropriate tracer-kinetic model to analyze the delivery of the contrast agent to the kidney(s).

Patient preparation

Basic patient preparation includes suitable hydration of the child, dose and timing of Lasix administration and the placement of a bladder catheter. These details have been described in previous papers and the interested reader is referred to these [26, 43]. It should be emphasized that having consistent hydration for all patients is a key factor in obtaining reliable and reproducible results. As detailed later in the “Feed-and-wrap method” section, these techniques can be used in infants. However, once children have grown beyond infancy, sedation is generally required until they are about 7 years of age. The basic MR urography protocol is outlined in Table 1.

Dynamic contrast-enhanced magnetic resonance imaging acquisition

Several techniques have been developed to measure the DRF with MRI by using the area under the time-intensity curve obtained from either a single slice, or a few slices, with a separate volume measurement [10, 27, 44,45,46]. However, to accurately estimate the GFR 3-D MRI images, high temporal resolution and sufficient spatial resolution are required. Dynamic contrast-enhanced MR images are most commonly acquired with Cartesian (rectangular) k-space sampling using T1-weighted fat-saturated three-dimensional (3-D) spoiled gradient echo (GRE) sequences. These are generally combined with parallel imaging to improve the temporal resolution, but at the expense of reduced signal-to-noise ratio. Depending on the size, number and configuration of the coils, the field strength of the magnet, the desired spatial resolution and the required coverage (field of view), the time for each dynamic volume can typically be reduced to somewhere in the range of 5–10 s. More recently, compressed sensing has been introduced as an alternative form of acceleration and quite high acceleration factors can also be obtained using this approach, but generally at the expense of lengthy reconstruction times. While these methods allow for excellent visualization of the passage of the contrast agent through the vasculature and the kidneys, the time to acquire each dynamic volume is generally too long to be able to accurately characterize the arterial input function if a compact bolus is used (which is an assumption of most models of renal function). As a result, many groups use a slower injection of contrast, which, while not ideal for tracer kinetic modeling, still allows modeling to be performed but with the caveat that the values obtained are “institutional values” (i.e. reproducible with the given patient preparation and the imaging sequence used) rather than quantitative values that can be compared with the results from other modalities. It should also be emphasized that regardless of the imaging technique used, consistent values can only be obtained when children are consistently well hydrated.

Another limitation of conventional Cartesian imaging is the sensitivity to motion, which reduces the quality of images, causing motion artifacts, and results in misalignment between the volumes in a dynamic series, complicating post-processing. Non-Cartesian sampling with radial imaging techniques such as BLADE and MultiVane have been familiar for many years as a means of reducing motion artifacts, but until recently these were restricted to 2-D acquisitions. The recent development of continuous golden angle radial sampling using a dynamic stack-of-stars sequence and parallel imaging in combination with compressed sensing have allowed motion insensitive, artifact-free 3-D dynamic series of volumes to be acquired. As with the 2-D radial sequences, all of the radial lines include the center of k-

space, making the sequence robust with respect to motion and offering the potential benefit of retrospective self-gating, thus eliminating the need for navigator signals or external devices [47]. Although radial MRI acquisition is inherently motion-robust compared to Cartesian MRI for shallow breathing, heavy-breathing motion and bulk motion can still significantly degrade the quality of the reconstructed images. Recent techniques have used motion detection and removal during image reconstruction to address this problem [48]. View sharing, where some lines of data are used for two or more different dynamics, can be used to improve the temporal resolution or to construct multiple data sets with differing temporal resolutions, but it can reduce the fidelity of the measurement of the arterial input function. A typical dynamic contrast-enhanced sequence starts by acquiring several pre-contrast images, to allow for a robust estimation of the pre-contrast signal, prior to a bolus injection of contrast agent being administered using a power injector; the sequence then continues for a minimum of 5 min and preferably 8–10 min. This allows the flow of the contrast agent into the renal cortex, the medulla and the collecting system to be visualized, allowing the physician to evaluate the uptake and excretion of contrast agent and to observe features such as the renal vessels, scarring, asymmetrical uptake and concentration of the contrast agent.

Motion correction and segmentation of the kidneys

The first step of postprocessing dynamic contrast-enhanced MR images is to determine whether motion correction is required. In our experience, sedated children ages 3 months to approximately 5 years show very little motion if the sedation is effective. If the motion consists primarily of displacement/distortion of the kidneys, then one of a number of techniques can be applied to try to register (align) the images [49, 50]. In cases where significant degradation of the image has also occurred, then motion correction is of little help. If only a few time-points are affected, then these can be discarded and the rest of the time-points can be registered. If large numbers of time-points are degraded, then it is not possible to process the data.

Following successful motion correction and segmentation of each kidney (or compartment), an arterial input function is derived using either a region of interest (ROI) or by segmenting the aorta [51]. For the aorta, care must be taken to avoid regions where in-flow artifact can distort the arterial input function. Inflow artifact can also be minimized by placing the kidneys in the middle of the of the field of view in coronal plane during acquisition. Either semi-automated or automated methods can be used for segmentation of the kidneys. Semi-automated methods require user input including 3-D region-of-interest selection, and these models often require manual refinement of segmentation and take more time to use. Fully automated segmentation methods do not require user input but might still need manual refinement of the segmentation mask, especially for abnormal kidneys (e.g., hydronephrosis) [51, 52]. Generally, the segmentation assumes that voxels represent either functional or non-functional tissue, and hence if there are regions with very poor function these might be excluded from the segmentation. By summing the voxels that show a significant uptake of contrast agent, one can calculate the functional volume of each kidney and hence derive both the volumetric differential renal function (vDRF) and the time–intensity curve for each kidney. To calculate the vDRF, the dynamic series are visually inspected to determine the

volume of the contrast agent that is first seen in the collecting system of each kidney; the volume prior to this is then used to calculate the functional volume of each kidney. In this way, differences in the time of excretion between the two kidneys are accounted for and it is not necessary to assume a particular time point, or range of times, for the calculation of vDRF. This approach has two advantages: the ability to separate renal parenchyma from the contrast agent excreted into the collecting system, and the ability to choose the optimal time point for measuring renal volume for each kidney. This is an advantage over renal scintigraphy, which uses fixed time points to calculate the DRF. Experience with MR urography has shown us that not all kidneys enhance to the same degree or at the same rate, particularly in children with obstructed kidneys.

Conversion of the magnetic resonance signal to concentration of the contrast agent

One of the main issues for MRI is that, unlike nuclear medicine or CT, the signal changes observed with MRI do not directly reflect the concentration of the contrast agent. In MRI, the contrast agent acts by changing the T1 and T2 relaxation times of the protons, which in turn leads to a change in signal. However, while the relationship between the change in either T1 or T2 is linearly related to the contrast agent concentration, the change in signal is only linear under certain conditions. In dynamic contrast-enhanced sequences, gradient echoes are widely used so the measured signal reflects changes in T1 and T2* (with the latter including the effects of both T2 and inhomogeneities in the magnetic field). However, because the echo times are generally very short, the signal changes caused by T2* can generally be ignored and hence the observed signal changes are considered to be the result of changes in the T1 relaxation time. Because tracer kinetic modeling requires a measurement of the concentration of the contrast agent, two main approaches have been used to achieve this:

(1) Aim to keep the relationship between the contrast agent concentration and the signal linear, which puts restrictions on the pulse sequence parameters and the peak concentration of the contrast agent. When this approach is used, the concentration versus time curves are simply calculated by subtracting the pre-contrast (baseline) signal from the measured signal at each time point, or alternatively dividing the subtracted signal by the baseline signal to give a value that is more consistent between studies. Some groups have used reduced doses of contrast agent to stay with the linear range, but care has to be taken not to reduce the effect of the contrast agent too much because this reduces the diagnostic value of the dynamic and post-contrast images.

(2) Use the MR signal to calculate the relaxation time. One approach for this method is to perform an additional sequence prior to contrast agent injection, which is used to measure the pre-contrast T1 relaxation time. An estimation of T1 can be done fairly rapidly, but a measurement that is accurate across the full range of relaxation times is more challenging, and accurately measuring T1 in the presence of flow is particularly challenging. Alternatively, literature values for the appropriate field strength and age of the child can be used.

The baseline T1 value, together with the measured signal changes and the pulse sequence parameters, can then be used to calculate the contrast agent concentration for each dynamic

volume. One other known, but little discussed, problem with this approach is that the relationship between the contrast agent concentration and the relaxation time depends on the relaxivity of the contrast agent. Typically, the value determined by the manufacturer of the contrast agent is used and this is generally measured in the laboratory using samples of blood plasma. While this is an appropriate measurement for the contrast agent concentration in the blood, the validity of this value for renal tissue is debatable, and at least one study has shown very different values for the relaxivity of renal tissues [53].

Tracer kinetic models

After the time–intensity curves from each kidney and the aorta have been converted to concentration versus time curves, they can be used as the input for the tracer kinetic model. The tracer kinetic model aims to replicate the mechanism of filtration, concentration and excretion in the kidneys. One important element in dynamic contrast-enhanced MRI is the selection of an appropriate tracer kinetic model from which the functional parameters can be estimated. The various tracer kinetic models aim to simulate some or all of the following processes: filtration of contrast in the glomerulus, without tubular secretion or reabsorption, followed by its extraction into the tubules in the cortex and passage through the loop of Henle in the renal medulla, and its transit out of the tubular compartment. When modeling this passage of contrast agent from the renal arteries into the kidney compartments, many assumptions are made that affect the accuracy of the calculated parameters.

Several tracer kinetic models are used in estimating functional parameters, including simple clearance models and more accurate tracer kinetic models [54, 55]. The Patlak model is a two-compartmental model that uses a linear fit and is widely employed because of its simplicity and robustness. However, it has two main limitations: (1) it is restricted to the vascular and tubular compartments and ignores the transit of the contrast agent out of the tubular compartment and (2) it assumes the vascular concentration of the contrast agent is in a steady state (i.e. well mixed). These restrictions make the Patlak model strongly dependent on the selection of the time interval over which the linear fit is calculated, and this can lead to reduced reproducibility of the calculated parameters [56]. Annet et al. [57] refined this model and introduced the delay and dispersion of the bolus between the aorta and renal vasculature and also considered the excretion of contrast agent from the renal tubules. Sourbron et al. [58] further extended this model to measure both renal perfusion and GFR. Three-compartment models developed by Lee et al. [59] and Zhang et al. [60] described structures in the cortex and medulla as serially connected compartments, but they required segmentation of the cortex and medulla to provide time–intensity curves for each compartment, which can be problematic in diseased kidneys. In addition, the increased number of parameters increases the complexity of the fitting, and while a good fit is always obtained, the reliability of the estimated value for each component tends to be lower, and the value obtained is often influenced by the initial values chosen for the parameters at the start of the fitting. In general, we prefer to follow the principle of Occam’s razor and use either the Patlak or two-compartment models for the tracer kinetic model. In this paper, we focus on the use of the Patlak and Annet models.

Accurate tracer kinetic modeling requires an accurate measurement of the arterial input function in the aorta. The arterial input function is characterized by a short-lived peak value, and subsequently a longer washout period. As discussed, high temporal resolution is required to accurately characterize the short-lived peak, but the measurement of the arterial input function is also affected by a number of other factors including in-flow effects, dephasing, flow pulsation, partial volumes and a nonlinear relationship between the concentration of the contrast agent and T1 at high concentrations of the contrast agent. For instance, the inflow of blood with full magnetization can lead to significant variation in the arterial input function measured at different positions along the aorta [55, 61]. Other studies have shown that the arterial input function is influenced by both the size and location of the ROI used to measure the arterial input function [62, 63]. An alternative method of obtaining an arterial input function is to use a population-averaged arterial input function obtained from a group of subjects; however, this method assumes a relatively homogeneous population (e.g., similar ages) and standardized injection protocol and ignores weight-dependent variations in the administered dose of contrast agent. It also ignores the dependence of the arterial input function on the cardiac output of the patient [61, 64]. A recent study adjusted a population-based arterial input function to each patient by estimating the cardiac output from the full width at half-maximum of the first pass of the arterial input function and the dose from the amplitude of the arterial input function [65]. However, this method still relies on the quality of the measured arterial input function and the assumptions used in the calibration to the individual patient.

Feed-and-wrap magnetic resonance imaging

Given the risks of sedatives and anesthetics on the growing brain, feed-and-wrap (swaddle) imaging of infants younger than 6 months is an important alternative that was first introduced for brain imaging and has proved successful for MR urography [2, 48, 66,67,68,69,70]. Although the concept is simple — the infants are fasted until the MRI, planned around nap time, and are then fed and swaddled until drowsy — the details are crucial for success. Leaving ample time for the process to unfold, a comfortable environment for the parent and child, and nurses and staff who are dedicated to this process are invaluable. Immobilization devices such as vacuum bags and body cushions and earmuffs for noise attenuation are all helpful. Intravenous lines, hydration lines and Foleys are placed prior to feeding. We have found that the sleeping infant moves the least right after falling asleep, and thus we do our dynamic contrast-enhanced imaging at that time. For dynamic contrast-enhanced imaging, motion-robust free-breathing sequences such as StarVIBE (volumetric interpolated breath-hold examination) are important to counteract natural respiratory motion. When possible, post-processing methods can be used to further reduce the appearance of patient motion for correct calculation of function.

Magnetic resonance urography interpretation: visual and quantitative

Visual assessment of the MR images is the crucial first step in interpreting the study and provides the framework in which the functional parameters are analyzed. The kidneys should be visually assessed as normal or abnormal and, if abnormalities are present, whether they are unilateral or bilateral. The visual information establishes an initial diagnosis that

can be both verified and quantified by the functional parameters. No single parameter is diagnostic; only by integrating the functional data with the visual assessment can a comprehensive diagnosis be achieved. The first steps are to assess the quality of the kidneys and identify when the contrast agent is excreted. The functional parameters used in MR urography are described in Table 2.

Visual evaluation of renal parenchyma

The quality of the renal parenchyma is assessed both on high-resolution T2-weighted images and during the parenchymal phase of the nephrogram. The renal parenchyma is typically classified as normal or dysplastic/uropathic (Figs. 1 and 2). The diagnosis of dysplasia is a histological one, and both dysplasia and uropathy look similar on MR images [71]. On T2-weighted images, signs that indicate underlying uropathic/dysplastic parenchyma and permanent renal damage include decrease in renal size, architectural disorganization with loss of corticomedullary differentiation, small subcortical cysts and parenchymal thinning with low cortical T2 signal intensity. The nephrogram in these cases usually shows weak, inhomogeneous contrast enhancement reflecting damage to the microvasculature as well as the glomeruli and tubules. The decrease in enhancement in the nephrographic phase can be caused by acute changes in GFR or more chronic changes associated with uropathy or evolving renal injury. These imaging findings reflect the histological changes of renal damage based on reduced glomerular number, glomerular hyalinization, cortical cysts and interstitial inflammation and fibrosis [72, 73]. The preoperative diagnosis of uropathy/dysplasia is important because these changes are permanent and are not amenable to surgical correction. The normal medulla is brighter than the cortex on T2-weighted images and shows increased signal intensity in the late parenchymal phase of contrast enhancement. Medullary volume loss can range from mild to severe. Longstanding hydronephrosis is characterized by medullary volume loss, and in cases of severe hydronephrosis the renal medulla is not discernible on routine MR urography.

Quantitative measures of renal function

Calyceal transit time and renal transit time—The two semi-quantitative measures of renal function are CTT and RTT. They are estimated by visual inspection of the dynamic contrast-enhanced images. The CTT is defined as the time it takes for contrast agent to pass from the cortex in the arterial phase to the dependent portions of the calyces on maximum-intensity projection (MIP) images of the dynamic post-contrast sequences [1]. In normal kidneys, CTT is symmetrical (Fig. 1). However, CTT is delayed in physiologically significant obstruction, hypotension, renal artery stenosis and dehydration (Fig. 3). Rapid CTT is usually a result of renal damage leading to a tubular concentrating defect (Figs. 4 and 5) but occasionally occurs in cases of glomerular hyperfiltration (Fig. 6). The mechanisms that influence the CTT might compete when complex pathology is present. After identifying evidence of significant medullary volume loss or uropathy/dysplasia on the T2 images, the CTT would be expected to be rapid when compared with the normal contralateral kidney. If the CTT is symmetrical or delayed in a child with significant medullary volume loss or uropathy/dysplasia, co-existent obstruction should be considered. In cases of uropathy/dysplasia combined with obstruction, there are competing forces, with uropathy tending to make the CTT rapid while the obstruction tends to prolong the CTT. Both rapid and

delayed CTT can be caused by different abnormalities affecting the nephron, and the balance between these glomerular and tubular influences determines the ultimate appearance of the MR urogram. The functional analysis is used to help distinguish the different underlying pathologies that could produce a similar visual appearance of the MR urogram.

Initially, MR urography was used to evaluate hydronephrosis/urinary tract dilatation and obstruction by calculating the RTT, which is defined as the time it takes for the contrast agent to pass from the initial enhancement of the renal cortex until it is visualized in the ureter below the lower pole of the kidney. The RTT is a coarse and essentially qualitative measure of renal function. Although the RTT calculation is similar to diuretic renal scintigraphy for categorizing dilated systems, it has become apparent from high-resolution anatomical images that drainage from the renal pelvis is dependent on the site of insertion of the ureter into the renal pelvis. For drainage to occur down the ureter, the contrast agent has to reach the level of the UPJ. The ureteric insertion is variable and might be located high on the renal pelvis, anteriorly, or posteriorly on the renal pelvis [74]. The contrast agent macromolecule is heavier than water, resulting in layering of the contrast agent in the dependent portions of the kidney, especially when there is marked hydronephrosis and stasis. Some authors have suggested performing MR urography in the prone position to promote drainage down the ureter [75]. However, most of our patients with hydronephrosis are sedated, and prone positioning makes sedation more challenging. It is important to remember that the RTT can be delayed as a result of obstruction as well as dilatation and stasis. A prolonged renal transit time might simply indicate poor drainage, and the stasis of urine is often indicated by fluid levels within the renal pelvis and calyces. The RTT is most valuable when it occurs in less than 4 min, which demonstrates there is no significant obstruction.

Volumetric differential renal function, Patlak differential renal function and asymmetry index—The goal of functional renal imaging is to identify and quantitate irreversible renal damage and nephron loss, as well as potentially reversible hemodynamic changes. DRF has been the most widely used measure of renal function because absolute measurements remain technically challenging, although recent advances make absolute measurements possible [22]. Once the MR study has been post-processed, the parameters available for assessing the functional status of each kidney include the renal volumes, the Patlak numbers (both total and unit), the mean transit time and the signal intensity vs. time curves (Figs. 1, 2, 3, 4 and 5). By evaluating these parameters both in isolation and collectively, we can derive a comprehensive evaluation of renal function. As described in the technical section, dynamic contrast-enhanced MRI is used to calculate the differential renal function based on the volume of enhancing renal tissue (volumetric differential renal function, or vDRF) and the rate at which contrast agent is filtered and excreted by the kidney; this method indirectly measures glomerular filtration rate (Patlak differential renal function, or pDRF). Each kidney is evaluated independently and compared to the contralateral kidney. Several authors have shown that the calculation of differential renal function based on renal volume agrees well with the DRF calculated using nuclear medicine [9, 10, 14, 15]. Estimation of differential renal function is most useful when the abnormality is unilateral and the contralateral kidney can act as an internal control. Unfortunately, it is

of limited value in cases of bilateral renal disease. Absolute measures of renal function are needed to fully evaluate bilateral disease.

We consider both vDRF and pDRF as related but distinct measures of renal function. The volume of the kidney is stable in the short term. However, the GFR changes rapidly in response to physiological or pathological stimuli. The pDRF is a measure of the GFR for each kidney that can then be compared to the volume of the kidney and contrasted with the GFR of the contralateral kidney. The pDRF allows us to evaluate how the nephrons in each kidney are working. In our analysis, we used the renal volume for each kidney as a marker for nephron endowment and estimated the overall glomerular function of that kidney using the Patlak number. In fact, the ratio of the two provides a means of assessing the average function per unit volume for each kidney. Because renal function is determined not only by the nephron mass but also by the single-nephron GFR, it makes sense to consider regional GFR in units of mL/min/cm^3 [41]. The quality of the functioning renal parenchyma can be assessed using the ratio of Patlak number divided by the functioning renal volume. This is termed the unit Patlak value for each kidney and we have found this to be clinically useful for measuring renal function, particularly if a normal contralateral kidney is available for comparison. The asymmetry index is used to compare the unit Patlak values for each kidney and is an indicator of the degree of functional derangement between the two kidneys irrespective of size. The unit Patlak reflects both the number of glomeruli and the single-nephron GFR per centimeter cubed of renal tissue. The asymmetry index is simply the difference in unit Patlak divided by their sum. This index is potentially more useful than a conventional global GFR measurement because it also provides measurement of regional renal function regardless of size [41]. The average unit Patlak for our normal populations is (mean ± standard deviation) 0.41±0.11 mL/min/cm^3. When the pDRF and the vDRF are similar for both kidneys, the asymmetry index is close to zero. When the volumetric and Patlak values diverge, the difference can provide insights into acute changes of renal function, usually a potentially reversible change in the GFR. Increase in the Patlak/mL occurs with glomerular hyperfiltration, whereas decrease in Patlak/mL occurs in uropathy, with a decreased nephron number in acute obstruction and decreased renal perfusion in pathology such as renal artery stenosis.

Signal intensity versus time curves—The change in signal intensity, or concentration, versus time curves comprises an aortic curve as well as curves representing the passage of the contrast agent through each kidney. The signal intensity curves only represent signal changes in the renal parenchyma; any signal from the collecting system is excluded. They provide an overview of the MR urogram for each kidney. The curves describe the perfusion, concentration and excretion of the contrast agent over time (Figs. 1, 2, 3, 4, 5 and 6). Using these curves, the two kidneys can be easily compared and contrasted, which is especially helpful when one kidney is normal. The aortic curve is characterized by a sharp peak corresponding to the injection bolus and rapidly decreases as the contrast agent is filtered from the vascular compartment and excreted by the kidney. The normal renal curve begins just after the aortic peak and has an initial brisk upslope reflecting renal perfusion (contrast agent in the renal vasculature of each kidney). Shortly after this, there is a more gradual increase reflecting contrast agent in the nephron secondary to ongoing glomerular filtration

as well as residual contrast agent in the renal vasculature. As 20% of the contrast agent is filtered at each pass through the kidney, the contrast agent concentration in the aorta decreases while that in the kidney increases. Over time the medulla enhances to the point where the contrast agent concentration is always higher than that of the cortex in normal kidneys. The increase within the medulla reflects reabsorption of water in the distal nephron resulting in the contrast agent becoming more concentrated. After the peak concentration, contrast agent washes out of the nephron into the calyces and collecting system; a steady state is then reached where the slope of the renal curve parallels that of the aorta.

Mean transit time—As mentioned, the urine tubular flow rate depends in large part on the GFR, which is regulated by the tubuloglomerular feedback and the myogenic mechanism [38]. Using the two-compartment Annet model, we can evaluate tubular function by calculating the MTT. In the Annet model, the second compartment represents the distribution of the contrast agent over the tubular system and can be used to estimate the MTT of the tubular system. The MTT is a particularly robust measure in normal kidneys under the correct hydration protocol. In an unpublished study of 38 children with normal-appearing kidneys on MR urography (i.e. 76 kidneys), the MTT was 53.9 s with a standard deviation of 9.4 s (J. D. Grattan-Smith, unpublished data). The MTT is independent of kidney volume but does increase slightly with age. The MTT was also shown to be another potentially reversible parameter when evaluating hydronephrosis and obstruction. In a group of 37 children with unilateral decompensated UPJ obstruction, the average preoperative MTT for the hydronephrotic kidney was 149 s with a standard deviation of 88 s (J. D. Grattan-Smith, unpublished data) (Fig. 7). Following successful pyeloplasty, the average MTT fell to 47.8±14 s. As the MTT increased, the obstruction appeared more severe. The relatively faster postoperative MTT was thought to represent an underlying concentration defect from medullary and tubular damage. The MTT for the normal contralateral kidneys in this group was 48±14 s preoperatively and 59±9 s postoperatively. This change might reflect a response to the relief of the contralateral UPJ obstruction (J. D. Grattan-Smith, unpublished data). The MTT is prolonged in children who are inadequately hydrated, so reproducible results are dependent on meticulous attention to hydration. Because the MTT is another potentially reversible parameter to evaluate the hemodynamic changes associated with obstruction, it can play a particularly helpful role in characterizing the severity of obstruction and is particularly helpful in children with bilateral hydronephrosis.

Patterns of disease—Several patterns have been described in various renal diseases including an obstructive pattern with a delayed and dense nephrogram (Fig. 3), a uropathic pattern where there is perfusion but little concentration of the contrast agent (Fig. 2) and a concentration defect pattern when the initial slope of the curve mirrors the normal side but has less amplitude and earlier washout from the parenchyma (Figs. 4 and 5). Occasionally we see a curve that is interpreted as glomerular hyperfiltration, where the entire curve is shifted to the left, with an earlier peak intensity and increased amplitude (Fig. 6). Because concentration defects and glomerular hyperfiltration can result in rapid CTTs, the curves are very helpful in differentiating between these distinct pathologies — one occurring at the level of the glomerulus and the other in the distal tubule of the nephron. A summary of the MR urography parameters in various physiological states is summarized in Table 3.

Common indications for magnetic resonance urography

The most common indications for MR urography in children are the evaluation of congenital anomalies of the kidney and urinary tract including hydronephrosis, renal malformations, uropathy and renal dysplasia as well as the identification of ectopic ureters in children with incontinence. Accurate functional evaluation in these children is essential to guide their clinical management. MR urography allows a more nuanced approach to these renal diseases because, in addition to estimating the overall renal mass, it can assess potentially reversible hemodynamic and pathophysiological changes that occur in response to obstruction. With MR imaging we have two related but distinct measures of potentially reversible renal function — the pDRF and the MTT.

Congenital urinary tract dilation (hydronephrosis)

The most common indication for MR urography in pediatric urology is the evaluation of urinary tract dilatation (hydronephrosis), which is usually detected antenatally. Congenital urinary tract dilatation can be transient, stable or lead to progressive renal damage. Although UPJ obstruction is the most common cause of congenital urinary tract dilatation, imaging is required to differentiate UPJ obstruction from other causes of urinary tract dilatation such as transient and functional urinary tract dilatation, ureterovesical junction (UVJ) obstruction and vesicoureteral reflux (VUR). Many children with congenital urinary tract dilatation have stable renal function and there is a relatively high rate of spontaneous resolution. Management is now focused on serial monitoring of the urinary tract dilatation and function in hopes of identifying children for whom surgery would improve or preserve renal function [76]. Congenital urinary tract dilatation remains a clinical conundrum, and criteria for surgical correction of upper tract obstruction are poorly established [77]. To highlight the value of quantitative functional MR imaging of the kidney, we focus here on UPJ obstruction.

Ureteropelvic junction obstruction is a partial or intermittent blockage of the flow of urine that repetitively causes the upper tracts to overfill and exceed their physiological capacity [78]. The high-volume overstretching results in pathologically high intra-pelvic pressures, which induce compensatory mechanisms such as suppression of urine production to reduce the pelvic pressures to normal. The physiological changes used to reduce urine production include decreasing the GFR and increasing water reabsorption from the distal nephron. To identify physiologically significant urinary tract obstruction, quantitative measures of renal function would ideally be performed during overdistention of the renal pelvis. On MR urography, these physiological changes can be identified as a decrease in the unit Patlak and increase in the MTT, which result in the classic delayed and dense nephrogram indicating obstruction. The longer the MTT and the larger the asymmetry index, the more severe the obstruction.

In our protocols, the hydronephrotic kidney is given a “stress test” aimed at over-distending the capacity of the upper tracts with a fluid load and administration of a diuretic 15 min before the contrast agent is administered [1]. It is important to remember that this might not be sufficient to trigger all obstructions. A useful concept when analyzing MR urograms is to visually define hydronephrosis as either compensated or decompensated in response

to the diuretic and fluid challenge [26, 79] (Figs. 1, 3 and 4). In a child with unilateral hydronephrosis, if there are symmetrical changes in the intensity of the nephrogram and symmetrical or rapid CTT, it is classified as a compensated hydronephrotic system — the fluid challenge has been accommodated without increasing the pressure in the pelvicalyceal system. However, when the signal intensity changes are asymmetrical and the calyceal transit time is delayed, they most often indicate acute-on-chronic obstruction — the fluid challenge has exceeded the capacity for renal drainage and the pressure in the collecting system rises. These are classified as decompensated hydronephrotic systems.

A similar observation has been made using renal scintigraphy. Using diuretic renal scintigraphy, some authors have used the cortical transit time — defined as the absence of activity in the subcortical structures within 3 min of tracer injection on diuretic renogram — to predict functional deterioration [80,81,82,83,84,85,86]. Delayed cortical transit has been predictive of DRF improvement postoperatively and it seems to be the best criterion for identifying children for whom pyeloplasty is warranted. Delayed parenchymal transit as a marker of urinary tract obstruction was first described by Whitfield et al. [87] in 1978 but diuretic renal scintigraphy is limited by its poor spatial resolution and has been unreliable when trying to separate renal parenchyma from collecting system, especially in markedly hydronephrotic systems [82, 87].

While the volumetric DRF is stable, the Patlak DRF can change rapidly in response to pathophysiological stimuli, resulting in decompensated hydronephrosis [26, 79]. The increased pressure in the renal pelvis is transmitted in a retrograde fashion throughout the nephron [88,89,90]. The increased pressure in the nephron extends across the Bowman space and results in prolonged transit of the contrast agent from the glomerulus to the collecting system. Glomerular filtration continues but at a reduced rate, probably through tubuloglomerular feedback and the myogenic mechanism [38, 91]. The tubular system continues to reabsorb electrolytes and fluid but does not resorb the contrast agent. These changes lead to the classic delayed and dense nephrogram, indicating obstruction. The discrepancy between the vDRF and pDRF is one way to quantitate the degree of obstruction, as measured through the asymmetry index. Studies following pyeloplasty have shown that the decrease in the pDRF is reversible and resolves after successful pyeloplasty [92] (Fig. 4). Decrease in pDRF compared to vDRF also occurs with unilateral renal artery stenosis and renal vein thrombosis.

Mean transit time is also prolonged in physiologically significant obstruction, which is manifested visually by delayed CTT. The MTT can quantitate the severity of obstruction, being markedly prolonged in cases of severe obstruction. The MTT is also a measure of reversible renal function because the MTT becomes more rapid following successful pyeloplasty. In these cases, the rapid MTT is secondary to an underlying concentration defect resulting from tubular and medullary damage. This is challenging when there is possible obstruction of a uropathic kidney because there are competing influences with rapid excretion from damaged nephrons and delayed excretion from increased intrapelvic pressure.

Duplex kidneys

Another common clinical indication for MR urography is the evaluation of duplex kidneys, especially duplex kidneys with complete ureteral duplication. The goal of treatment is preservation of renal function and relieving clinical symptoms, such as recurrent urinary tract infections or incontinence. Because the management of duplex, ectopic and fused kidneys depends on an understanding of the anatomy, the function of each moiety and degree of obstruction, MR urography is the single best test to answer these questions [10, 13, 27, 93,94,95]. In duplex kidneys with either upper- or lower-pole dilation, the management is based on the presence of reflux, the degree of obstruction, the function of each moiety, and the site of ureteral insertion. The dilated moiety that is obstructed or has decreased function is more likely to be repaired surgically than dilated moieties without obstruction and with maintained function. In the evaluation of duplex kidneys, MR urography can separate the boundaries between the upper and lower poles by delineating the column of cortex separating the poles so that the relative contributions of each pole can be calculated (Fig. 8). Surgical approaches differ by surgeon but are based on the functional information provided by the MR urogram. For example, the degree of function in the upper moiety can alter the surgical approach from a ureteroureterostomy to a partial upper pole nephroureterectomy. MR urography is also helpful in distinguishing anatomically complex duplex anomalies or the mimics of duplex collecting systems, such as cysts, calyceal diverticuli and multicystic dysplastic kidneys.

Conclusion

Magnetic resonance urography has evolved into a comprehensive test that combines high-resolution anatomical imaging with quantitative measures of renal function. MR urography characterizes the changes in renal function that occur to compensate for nephron loss. MR urography has prognostic implications because the preoperative appearance and function of the kidneys can predict the outcome of pyeloplasty. MR urography allows a more nuanced interpretation of complex renal disease and has the potential to differentiate abnormalities related to glomerular filtration from those related to tubular function. MR urography is used to identify and quantify decompensated hydronephrosis through analysis of two potentially reversible function changes in both the pDRF and the MTT. Both these parameters return to normal following successful pyeloplasty. However, the importance of visual assessment of the images cannot be overstated when analyzing the quantitative measures of renal function. The complex pathophysiology of renal disease means that no single parameter can fully characterize renal disease.

References

1. Jones RA, Grattan-Smith JD, Little S (2014) MR urography in children. Springer, Milan, pp 295–310
2. Kurugol S, Seager CM, Thaker H et al. (2020) Feed and wrap magnetic resonance urography provides anatomic and functional imaging in infants without anesthesia. J Pediatr Urol 16:116–120 [PubMed: 31889687]
3. Bokacheva L, Rusinek H, Zhang JL et al. (2009) Estimates of glomerular filtration rate from MR renography and tracer kinetic models. J Magn Reson Imaging 29:371–382 [PubMed: 19161190]

4. Grenier N, Mendichovszky I, de Senneville BD et al. (2008) Measurement of glomerular filtration rate with magnetic resonance imaging: principles, limitations, and expectations. Semin Nucl Med 38:47–55 [PubMed: 18096463]
5. Sourbron S (2010) Compartmental modelling for magnetic resonance renography. Z Med Phys 20:101–114 [PubMed: 20540902]
6. Tofts PS, Cutajar M, Mendichovszky IA et al. (2012) Precise measurement of renal filtration and vascular parameters using a two-compartment model for dynamic contrast-enhanced MRI of the kidney gives realistic normal values. Eur Radiol 22:1320–1330 [PubMed: 22415410]
7. Grenier N, Merville P, Combe C (2016) Radiologic imaging of the renal parenchyma structure and function. Nat Rev Nephrol 12:348–359 [PubMed: 27067530]
8. Thomas SR (2019) Mathematical models for kidney function focusing on clinical interest. Morphologie 103:161–168 [PubMed: 31722814]
9. Claudon M, Durand E, Grenier N et al. (2014) Chronic urinary obstruction: evaluation of dynamic contrast-enhanced MR urography for measurement of split renal function. Radiology 273:801–812 [PubMed: 25102294]
10. Damasio MB, Bodria M, Dolores M et al. (2019) Comparative study between functional MR urography and renal scintigraphy to evaluate drainage curves and split renal function in children with congenital anomalies of kidney and urinary tract (CAKUT). Front Pediatr 7:527 [PubMed: 32047727]
11. Khrichenko D, Saul D, Adeb M et al. (2016) Intra- and inter-observer variability of functional MR urography (fMRU) assessment in children. Pediatr Radiol 46:666–673 [PubMed: 26795619]
12. Morin CE, McBee MP, Trout AT et al. (2018) Use of MR urography in pediatric patients. Curr Urol Rep 19:93 [PubMed: 30206713]
13. Rodigas J, Kirsch H, John U et al. (2018) Static and functional MR urography to assess congenital anomalies of the kidney and urinary tract in infants and children: comparison with MAG3 renal scintigraphy and sonography. AJR Am J Roentgenol 211:193–203 [PubMed: 29702016]
14. Cerwinka WH, Grattan-Smith JD, Jones RA et al. (2014) Comparison of magnetic resonance urography to dimercaptosuccinic acid scan for the identification of renal parenchyma defects in children with vesicoureteral reflux. J Pediatr Urol 10:344–351 [PubMed: 24128878]
15. Wong MCY, Sertorio F, Damasio MB et al. (2019) Surgical validation of functional magnetic resonance urography in the study of ureteropelvic junction obstruction in a pediatric cohort. J Pediatr Urol 15:168–175 [PubMed: 30553558]
16. Saxton HM (1969) Review article: urography. Br J Radiol 42:321–346 [PubMed: 4914357]
17. Dawson P (1990) Intravenous urography revisited. Br J Urol 66:561–567 [PubMed: 2265324]
18. Sherwood T (1971) The physiology of intravenous urography. Sci Basis Med Annu Rev 1971:336–348
19. Grattan-Smith JD, Perez-Bayfield MR, Jones RA et al. (2003) MR imaging of kidneys: functional evaluation using F-15 perfusion imaging. Pediatr Radiol 33:293–304 [PubMed: 12695861]
20. Grattan-Smith JD, Jones RA (2008) MR urography: technique and results for the evaluation of urinary obstruction in the pediatric population. Magn Reson Imaging Clin N Am 16:643–660 [PubMed: 18926428]
21. Jones RA, Perez-Brayfield MR, Kirsch AJ, Grattan-Smith JD (2004) Renal transit time with MR urography in children. Radiology 233:41–50 [PubMed: 15317951]
22. Kurugol S, Afacan O, Lee RS et al. (2020) Prospective pediatric study comparing glomerular filtration rate estimates based on motion-robust dynamic contrast-enhanced magnetic resonance imaging and serum creatinine (eGFR) to 99mTc DTPA. Pediatr Radiol 50:698–705 [PubMed: 31984436]
23. Bokacheva L, Rusinek H, Zhang JL, Lee VS (2008) Assessment of renal function with dynamic contrast-enhanced MR imaging. Magn Reson Imaging Clin N Am 16:597–611 [PubMed: 18926425]
24. Khrichenko D, Darge K (2010) Functional analysis in MR urography — made simple. Pediatr Radiol 40:182–199 [PubMed: 20012602]
25. Vivier P-H, Dolores M, Taylor M et al. (2010b) MR urography in children. Part 1: how we do the F0 technique. Pediatr Radiol 40:732–738 [PubMed: 20182706]

26. Jones RA, Grattan-Smith JD, Little S (2011) Pediatric magnetic resonance urography. J Magn Reson Imaging 33:510–526 [PubMed: 21563236]
27. Boss A, Martirosian P, Fuchs J et al. (2014) Dynamic MR urography in children with uropathic disease with a combined 2D and 3D acquisition protocol — comparison with MAG3 scintigraphy. Br J Radiol 87:20140426 [PubMed: 25270833]
28. Lowenstein J, Grantham JJ (2016) The rebirth of interest in renal tubular function. Am J Physiol Renal Physiol 310:F1351–F1355 [PubMed: 26936872]
29. Lumbers ER, Kandasamy Y, Delforce SJ et al. (2020) Programming of renal development and chronic disease in adult life. Front Physiol 11:757 [PubMed: 32765290]
30. Helal I, Fick-Brosnahan GM, Reed-Gitomer B, Schrier RW (2012) Glomerular hyperfiltration: definitions, mechanisms and clinical implications. Nat Rev Nephrol 8:293–300 [PubMed: 22349487]
31. Chevalier RL (2016) Prognostic factors and biomarkers of congenital obstructive nephropathy. Pediatr Nephrol 31:1–10 [PubMed: 25631241]
32. Chevalier RL (2014) The life cycle of the kidney: implications for CKD. J Am Soc Nephrol 25:2388–2390 [PubMed: 24812166]
33. Chevalier RL (2016) The proximal tubule is the primary target of injury and progression of kidney disease: role of the glomerulotubular junction. Am J Physiol Renal Physiol 311:F145–F161 [PubMed: 27194714]
34. Denic A, Elsherbiny H, Rule AD (2019) In-vivo techniques for determining nephron number. Curr Opin Nephrol Hypertens 28:545–551 [PubMed: 31433316]
35. Chawla LS, Ronco C (2016) Renal stress testing in the assessment of kidney disease. Kidney Int Rep 1:57–63 [PubMed: 29142914]
36. Ronco C, Chawla LS (2016) Glomerular and tubular kidney stress test: new tools for a deeper evaluation of kidney function. Nephron 134:191–194 [PubMed: 27577054]
37. Sharma A, Zaragoza JJ, Villa G et al. (2016) Optimizing a kidney stress test to evaluate renal functional reserve. Clin Nephrol 86:18–26
38. Layton AT (2012) Modeling transport and flow regulatory mechanisms of the kidney. ISRN Biomath 2012:170594 [PubMed: 23914303]
39. Nyengaard JR, Bendtsen TF (1992) Glomerular number and size in relation to age, kidney weight, and body surface in normal man. Anat Rec 232:194–201 [PubMed: 1546799]
40. Kim HC, Yang DM, Jin W, Lee SH (2010) Relation between total renal volume and renal function: usefulness of 3D sonographic measurements with a matrix array transducer. AJR Am J Roentgenol 194:W186–W192 [PubMed: 20093572]
41. Tsushima Y, Blomley MJ, Okabe K et al. (2001) Determination of glomerular filtration rate per unit renal volume using computerized tomography: correlation with conventional measures of total and divided renal function. J Urol 165:382–385 [PubMed: 11176378]
42. Bueters RR, van de Kar NC, Schreuder MF (2013) Adult renal size is not a suitable marker for nephron numbers: an individual patient data meta-analysis. Kidney Blood Press Res 37:540–546 [PubMed: 24356546]
43. Grattan-Smith JD (2008) MR urography: anatomy and physiology. Pediatr Radiol 38:275–280
44. Huang AJ, Lee VS, Rusinek H (2004) Functional renal MR imaging. Magn Reson Imaging Clin N Am 12:469–486 [PubMed: 15271366]
45. Vivier P-H, Dolores M, Taylor M, Dacher J-N (2010) MR urography in children. Part 2: how to use ImageJ MR urography processing software. Pediatr Radiol 40:739–746 [PubMed: 20182707]
46. Artunc F, Yildiz S, Rossi C et al. (2010) Simultaneous evaluation of renal morphology and function in live kidney donors using dynamic magnetic resonance imaging. Nephrol Dial Transplant 25:1986–1991 [PubMed: 20100730]
47. Riffel P, Zoellner FG, Budjan J et al. (2016) “One-stop shop”: free-breathing dynamic contrast-enhanced magnetic resonance imaging of the kidney using iterative reconstruction and continuous golden-angle radial sampling. Investig Radiol 51:714–719 [PubMed: 27299581]
48. Coll-Font J, Afacan O, Chow JS et al. (2020) Bulk motion-compensated DCE-MRI for functional imaging of kidneys in newborns. J Magn Reson Imaging 52:207–216 [PubMed: 31837071]

49. Coll-Font J, Afacan O, Chow JS et al. (2021) Modeling dynamic radial contrast enhanced MRI with linear time invariant systems for motion correction in quantitative assessment of kidney function. Med Image Anal 67:101880 [PubMed: 33147561]
50. Derle N, Dighe D (2012) 4D image analysis and diagnosis of kidney disease using DCE-MRI images. Int J Innov Res Sci Eng 2
51. Haghighi M, Warfield SK, Kurugol S (2018) Automatic renal segmentation in DCE-MRI using convolutional neural networks. Proc IEEE Int Symp Biomed Imaging 2018:1534–1537 [PubMed: 30473744]
52. Yoruk U, Hargreaves BA, Vasanawala SS (2018) Automatic renal segmentation for MR urography using 3D-GrabCut and random forests. Magn Reson Med 79:1696–1707 [PubMed: 28656614]
53. Mørkenborg J, Taagehøj JF, Vaever PN et al. (1998) In vivo measurement of T1 and T2 relaxivity in the kidney cortex of the pig — based on a two-compartment steady-state model. Magn Reson Imaging 16:933–942 [PubMed: 9814776]
54. Patlak CS, Blasberg RG (1985) Graphical evaluation of blood-to-brain transfer constants from multiple-time uptake data. Generalizations J Cereb Blood Flow Metab 5:584–590 [PubMed: 4055928]
55. Zhang JL, Lee VS (2020) Renal perfusion imaging by MRI. J Magn Reson Imaging 52:369–379 [PubMed: 31452303]
56. Hackstein N, Kooijman H, Tomaselli S, Rau WS (2005) Glomerular filtration rate measured using the Patlak plot technique and contrast-enhanced dynamic MRI with different amounts of gadolinium-DTPA. J Magn Reson Imaging 22:406–414 [PubMed: 16106358]
57. Annet L, Hermoye L, Peeters F et al. (2004) Glomerular filtration rate: assessment with dynamic contrast-enhanced MRI and a cortical-compartment model in the rabbit kidney. J Magn Reson Imaging 20:843–849 [PubMed: 15503326]
58. Sourbron SP, Michaely HJ, Reiser MF, Schoenberg SO (2008) MRI-measurement of perfusion and glomerular filtration in the human kidney with a separable compartment model. Investig Radiol 43:40–48 [PubMed: 18097276]
59. Lee VS, Rusinek H, Bokacheva L et al. (2007) Renal function measurements from MR renography and a simplified multicompartmental model. Am J Physiol Renal Physiol 292:F1548–F1559 [PubMed: 17213464]
60. Zhang JL, Rusinek H, Bokacheva L et al. (2008) Functional assessment of the kidney from magnetic resonance and computed tomography renography: impulse retention approach to a multicompartment model. Magn Reson Med 59:278–288 [PubMed: 18228576]
61. Parker GJ, Roberts C, Macdonald A et al. (2006) Experimentally-derived functional form for a population-averaged high-temporal-resolution arterial input function for dynamic contrast-enhanced MRI. Magn Reson Med 56:993–1000 [PubMed: 17036301]
62. Cutajar M, Mendichovszky IA, Tofts PS, Gordon I (2010) The importance of AIF ROI selection in DCE-MRI renography: reproducibility and variability of renal perfusion and filtration. Eur J Radiol 74:e154–e160 [PubMed: 19541441]
63. Mendichovszky IA, Cutajar M, Gordon I (2009) Reproducibility of the aortic input function (AIF) derived from dynamic contrast-enhanced magnetic resonance imaging (DCE-MRI) of the kidneys in a volunteer study. Eur J Radiol 71:576–581 [PubMed: 19004588]
64. Wang Y, Huang W, Panicek DM et al. (2008) Feasibility of using limited-population-based arterial input function for pharmacokinetic modeling of osteosarcoma dynamic contrast-enhanced MRI data. Magn Reson Med 59:1183–1189 [PubMed: 18429032]
65. Kim H (2018) Modification of population based arterial input function to incorporate individual variation. Magn Reson Imaging 45:66–71 [PubMed: 28958876]
66. Antonov NK, Ruzal-Shapiro CB, Morel KD et al. (2017) Feed and wrap MRI technique in infants. Clin Pediatr 56:1095–1103
67. Lin EP, Soriano SG, Loepke AW (2014) Anesthetic neurotoxicity. Anesthesiol Clin 32:133–155 [PubMed: 24491654]
68. Mellon RD, Simone AF, Rappaport BA (2007) Use of anesthetic agents in neonates and young children. Anesth Analg 104:509–520 [PubMed: 17312200]

69. Rappaport B, Mellon RD, Simone A, Woodcock J (2011) Defining safe use of anesthesia in children. N Engl J Med 364:1387–1390 [PubMed: 21388302]
70. Templeton LB, Norton MJ, Goenaga-Díaz EJ et al. (2020) Experience with a “feed and swaddle” program in infants up to six months of age. Acta Anaesthesiol Scand 64:63–68 [PubMed: 31506920]
71. Grattan-Smith JD, Little SB, Jones RA (2007) Evaluation of reflux nephropathy, pyelonephritis and renal dysplasia. Pediatr Radiol 38:83–105
72. Huang W-Y, Peters CA, Zurakowski D et al. (2006) Renal biopsy in congenital ureteropelvic junction obstruction: evidence for parenchymal maldevelopment. Kidney Int 69:137–143 [PubMed: 16374434]
73. Elder JS, Stansbrey R, Dahms BB, Selzman AA (1995) Renal histological changes secondary to ureteropelvic junction obstruction. J Urol 154:719–722 [PubMed: 7609162]
74. Kaneyama K, Yamataka A, Someya et al. (2006) Magnetic resonance urographic parameters for predicting the need for pyeloplasty in infants with prenatally diagnosed severe hydronephrosis. J Urol 176:1781–1785
75. Delgado J, Bedoya MA, Adeb M et al. (2015) Optimizing functional MR urography: prime time for a 30-minutes-or-less fMRU. Pediatr Radiol 45:1333–1343 [PubMed: 25792155]
76. Passoni NM, Peters CA (2020) Managing ureteropelvic junction obstruction in the young infant. Front Pediatr 8:242 [PubMed: 32537441]
77. Chevalier RL (2015) Congenital urinary tract obstruction: the long view. Adv Chronic Kidney Dis 22:312–319 [PubMed: 26088076]
78. Koff S (2019) The search for the definition and effective diagnosis of upper urinary tract obstruction: the Whitaker test then and now, Whitaker et al. 2018. J Pediatr Urol 15:27–28 [PubMed: 30528651]
79. Aaronson IA (1980) Compensated obstruction of the renal pelvis. Br J Urol 52:79–83 [PubMed: 7426970]
80. Schlotmann A, Clorius JH, Rohrschneider WK et al. (2008) Diuretic renography in hydronephrosis: delayed tissue tracer transit accompanies both functional decline and tissue reorganization. J Nucl Med 49:1196–1203 [PubMed: 18552148]
81. Schlotmann A, Clorius JH, Clorius SN (2009) Diuretic renography in hydronephrosis: renal tissue tracer transit predicts functional course and thereby need for surgery. Eur J Nucl Med Mol Imaging 36:1665–1673 [PubMed: 19437014]
82. Sfakianakis GN, Sfakianaki E, Georgiou M et al. (2009) A renal protocol for all ages and all indications: mercapto-acetyl-triglycine (MAG3) with simultaneous injection of furosemide (MAG3-F0): a 17-year experience. Semin Nucl Med 39:156–173 [PubMed: 19341836]
83. Piepsz A, Tondeur M, Nogarède C et al. (2011) Can severely impaired cortical transit predict which children with pelvi-ureteric junction stenosis detected antenatally might benefit from pyeloplasty? Nucl Med Commun 32:199–205 [PubMed: 21178646]
84. Harper L, Bourquard D, Grosos C et al. (2013) Cortical transit time as a predictive marker of the need for surgery in children with pelvi-ureteric junction stenosis: preliminary study. J Pediatr Urol 9:1054–1058 [PubMed: 23602207]
85. Duong HP, Piepsz A, Collier F et al. (2013) Predicting the clinical outcome of antenatally detected unilateral pelviureteric junction stenosis. Urology 82:691–696 [PubMed: 23726167]
86. Jain V, Kumar R, Arora S et al. (2020) Cortical transit time: understanding utility and pitfalls in children with pelviureteric junction obstruction. J Pediatr Urol 16:330.e1–330.e6 [PubMed: 32253148]
87. Whitfield HN, Britton KE, Hendry WF et al. (1978) The distinction between obstructive uropathy and nephropathy by radioisotope transit times. Br J Urol 50:433–436 [PubMed: 753492]
88. Brenes LG, Forlano H, Koutouratsas N, Stauffer HM (1966) Mechanism of the nephrographic effect during urinary stasis. Acta Radiol Diagn 4:14–20
89. Korobkin M (1972) Physiology and significance of the prolonged nephrogram. Calif Med 117:55–56
90. Dyer RB, Munitz HA, Bechtold R, Choplin RH (1986) The abnormal nephrogram. Radiographics 6:1039–1063 [PubMed: 3685518]

91. Anigstein R, Elkin M, Roland P, Schulz RJ (1972) The obstructive nephrogram — microradiographic studies. Investig Radiol 7:24–32 [PubMed: 4551067]

92. Little SB, Jones RA, Grattan-Smith JD (2007) Evaluation of UPJ obstruction before and after pyeloplasty using MR urography. Pediatr Radiol 38:106–124

93. Adeb M, Darge K, Dillman JR et al. (2013) Magnetic resonance urography in evaluation of duplicated renal collecting systems. Magn Reson Imaging Clin N Am 21:717–730 [PubMed: 24183522]

94. Avni FE, Nicaise N, Hall M et al. (2001) The role of MR imaging for the assessment of complicated duplex kidneys in children: preliminary report. Pediatr Radiol 31:215–223 [PubMed: 11321736]

95. Figueroa VH, Chavhan GB, Oudjhane K, Farhat W (2014) Utility of MR urography in children suspected of having ectopic ureter. Pediatr Radiol 44:956–962 [PubMed: 24535117]

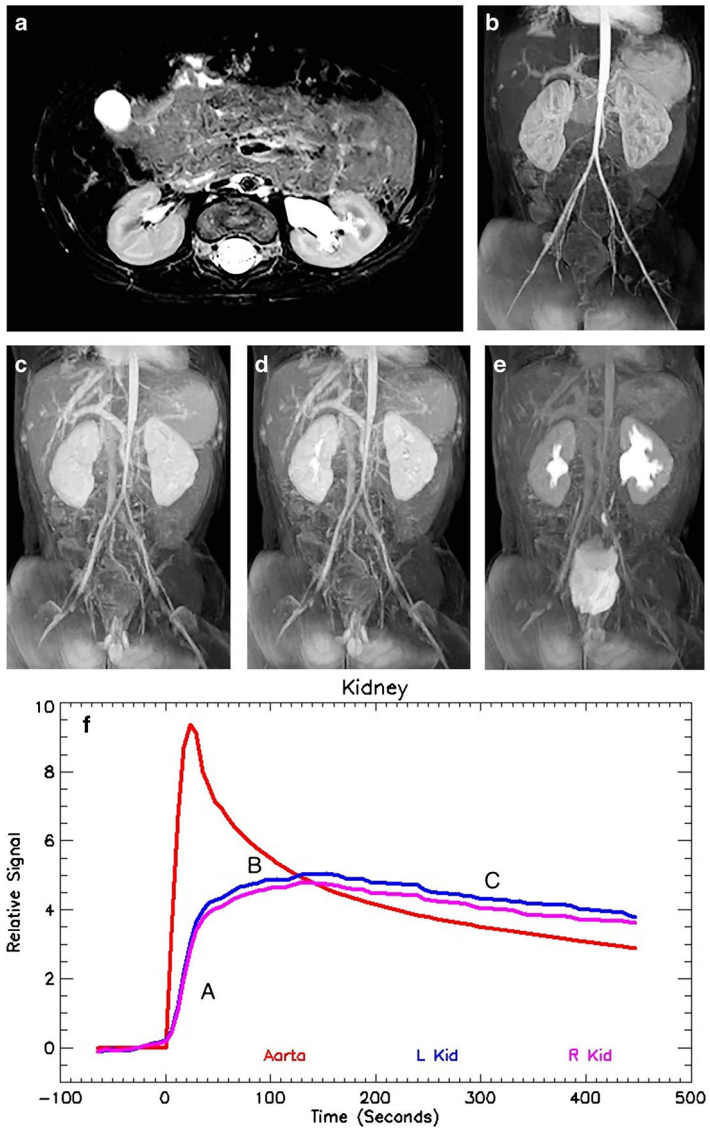

Fig. 1.

Magnetic resonance urogram in a 3-month-old boy with antenatal hydronephrosis. **a** Axial T2-weighted MR image shows mild dilatation of the left renal pelvis without caliectasis. The renal parenchyma appears normal, with preservation of the corticomedullary differentiation and normal increased signal intensity in the renal medulla. The assessment of the renal parenchyma is the first step in interpreting quantitative renal MR data. **b** Coronal post-contrast T1-weighted maximum-intensity projection (MIP) MR image derived from the early cortical phase shows contrast agent within the aorta as well as brisk and symmetrical enhancement of the renal parenchyma. The initial contrast enhancement of the kidneys occurs predominantly from renal perfusion, with the contrast agent localized to the vascular compartments of the kidneys. This is followed by gradual increase in parenchymal enhancement secondary to glomerular filtration of the contrast agent and tubular reabsorption of water. The renal outlines are smooth and the kidneys' size is similar. **c** Coronal post-contrast T1-weighted MIP image derived from the late nephrographic phase,

obtained 45 s later than the arterial phase seen in (**b**), demonstrates enhancement of both the cortex and medulla. The gadolinium concentration in the vascular compartment is decreasing while the contrast agent in the nephron is increasing and becoming more concentrated. The signal intensity of the medulla exceeds that of the cortex as a result of tubular concentration. **d** Coronal post-contrast T1-weighted MIP image acquired 60 s after the vascular phase shows initial excretion into the calyces. The appearance of the contrast agent in the calyces is essentially simultaneous, demonstrating no evidence of increased pressure in the renal pelvis. The mean transit time (MTT) on the right was 54 s and on the left 56 s, both within the normal range. The calyceal transit time (CTT) is a visual marker used in initial classification of a hydronephrotic kidney that can be quantified using the MTT. **e** Maximum-intensity projection image acquired 10 min after the initial vascular phase shows contrast agent filling the renal pelvis and ureters bilaterally. The right side is normal, with a renal transit time of 2 min 45 s. There is mild dilatation of the left renal pelvis with transition in caliber at the level of the ureteropelvic junction (UPJ) and a normal-size left ureter. The renal transit time on the left was slightly delayed when compared to the right, with contrast agent appearing in the left ureter at 3 min 30 s. This was in the normal range and no evidence suggested physiologically significant obstruction. **f** Normal signal intensity versus time curves for both kidneys demonstrate similar morphology reflecting the perfusion, concentration and excretion of the contrast agent. It is important to remember that the signal intensity curves represent only contrast agent within the renal parenchyma because any signal in the collecting system is excluded from the analysis. The red curve represents the signal in the aorta and is reflective of the contrast bolus with abrupt initial upstroke followed by an exponential decay curve. The initial upstroke of the curves for both kidneys (*A*) is related to renal perfusion. The flatter but still increasing second portion of the curve (*B*) represents glomerular filtration and tubular concentration of the contrast agent. Once the contrast agent begins to be excreted, there is a gentle decrease in the parenchymal contrast agent, paralleling the signal in the aorta (*C*). The quantitative measures of renal function were normal: vDRF L:R = 49:51; pDRF L:R = 48:52; unit Patlak L:R = 0.27:0.28 mL/min/cm^3; asymmetry index = 0.0; MTT, L=56 s, R=52 s. *L* left, *pDRF* Patlak differential renal function, *R* right, *vDRF* volumetric differential renal function

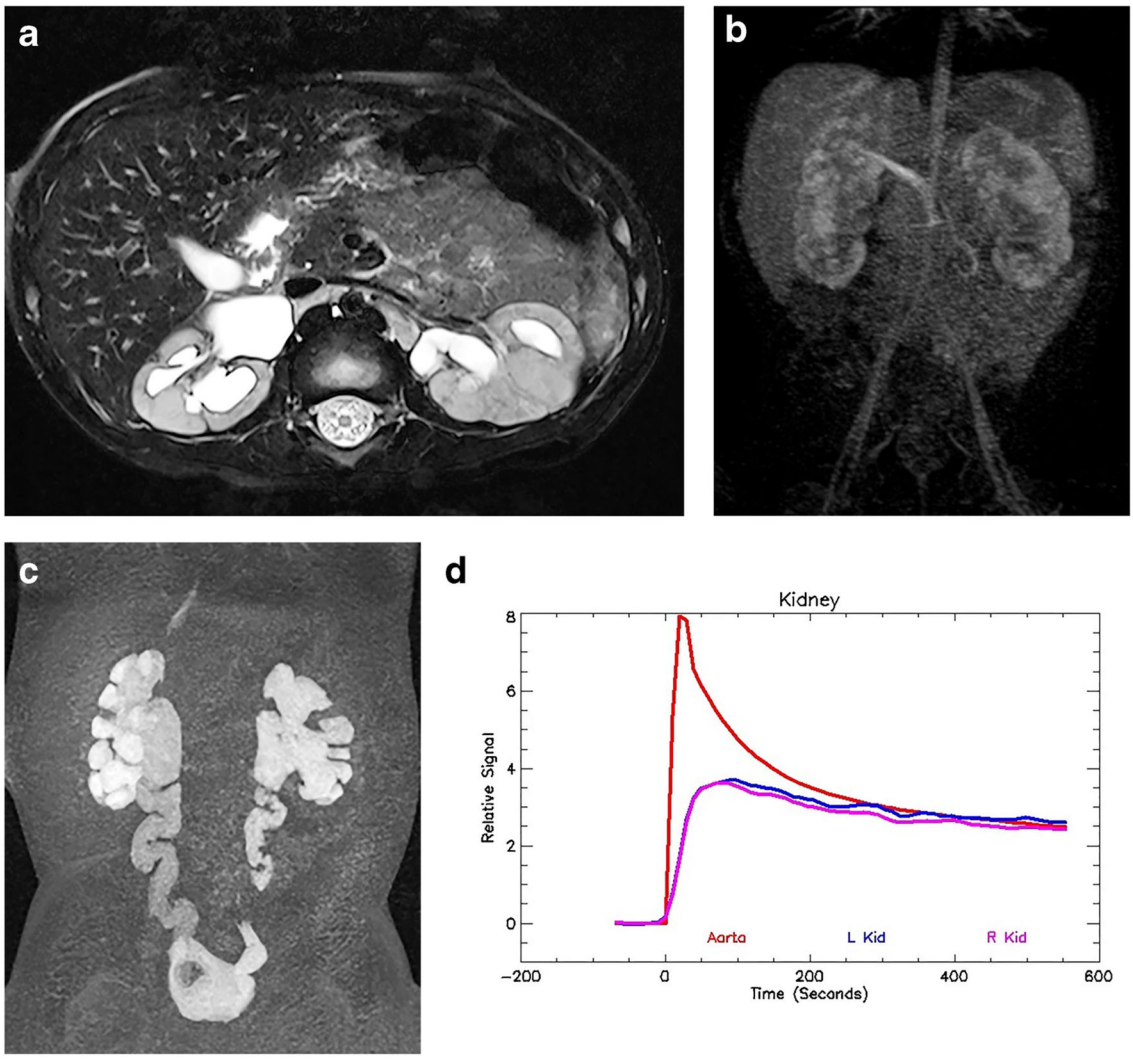

Fig. 2.

Bilateral renal dysplasia/uropathy and history of posterior urethral valves in a 1-year-old boy. **a** Axial T2-weighted MR image of both kidneys demonstrates mild hydronephrosis with irregular renal outlines and distortion of the renal architecture. There is no appreciable corticomedullary differentiation. **b** Coronal nephrographic phase after contrast administration shows bilateral irregular enhancement with no discernable concentration in the medulla. The nephrographic appearance reflects damage to the microvasculature as well as the glomeruli and tubules. **c** The delayed coronal post-contrast T1-weighted maximum-intensity projection (MIP) image shows bilateral hydroureteronephrosis with tortuosity of the ureters. The contrast agent eventually fills both urinary systems, although stasis and poor drainage are superimposed on the renal damage. **d** The signal intensity vs. time curve illustrates a normal aortic curve with bilateral dysplastic/uropathic curves for the kidneys. There is an initial brisk enhancement secondary to renal perfusion, with reduced glomerular filtration and no evidence of medullary concentration. The filtered contrast agent washed out from the renal parenchyma. The functional analysis was: vDRF L:R = 57:43; pDRF L:R = 55:45; unit Patlak L:R = 0.28:0.28 mL/min/cm^3; asymmetry index = 0.0; MTT, L=44 s,

R=40 s. *L* left, *MTT* mean transit time, *pDRF* Patlak differential renal function, *R* right, *vDRF* volumetric differential renal function.

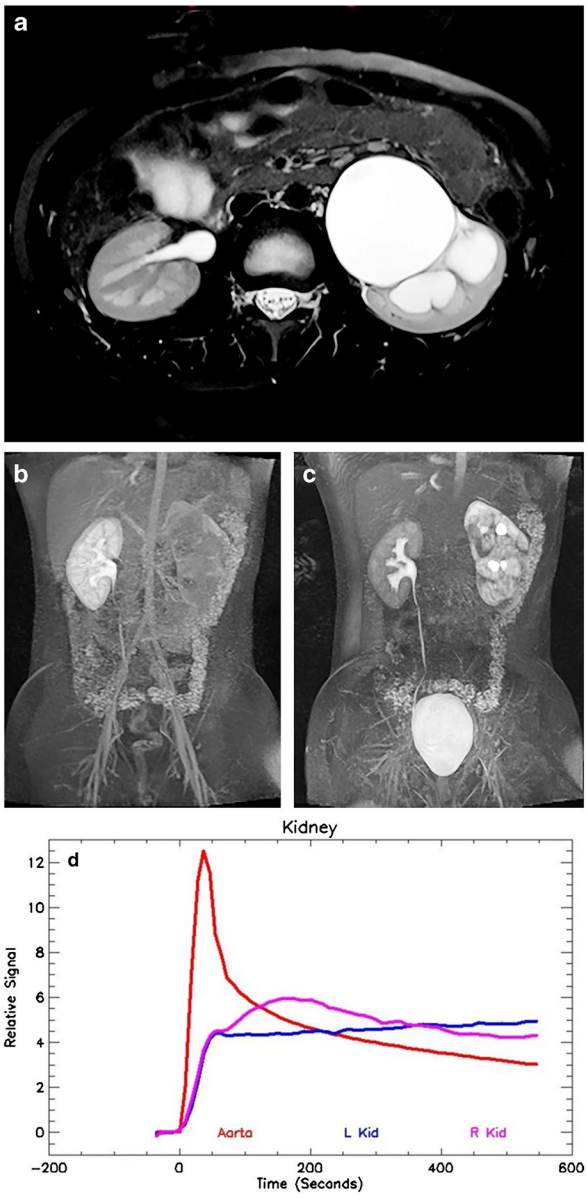

Fig. 3.

Decompensated ureteropelvic junction (UPJ) obstruction on the left in a 9-year-old boy. **a** Axial T2-weighted MR image shows marked dilatation and ballooning of the left renal pelvis and calyces. A small rim of medulla is still visible. Minor perinephric edema is also evident. The right kidney is normal. **b** Coronal late nephrographic phase maximum-intensity projection (MIP) image shows normal right kidney with prompt excretion. The left kidney has a markedly delayed and heterogeneous nephrogram. **c** Coronal delayed MIP shows the irregular renal outline on the left, with patchy nephrogram that is increasingly dense when compared with the normal right kidney. The increasing density is caused by a reduced glomerular filtration rate (GFR) and increased tubular reabsorption of water — the physiological responses that mitigate the effects of increased intra-pelvic pressure secondary to acute obstruction. **d** Signal intensity versus time curves show normal aortic

and right kidney curves. The left kidney demonstrates an obstructive pattern curve with brisk enhancement secondary to renal perfusion followed by a slow and persistent increase in signal intensity reflecting parenchymal retention of the contrast medium. The renal functional analysis was: vDRF L:R = 45:55; pDRF L:R = 36:64; unit Patlak L:R = 0.12:0.21 mL/min/cm^3; asymmetry index = 0.26; MTT, L=147 s, R=54 s. *L* left, *MTT* mean transit time, *pDRF* Patlak differential renal function, *R* right, *vDRF* volumetric differential renal function

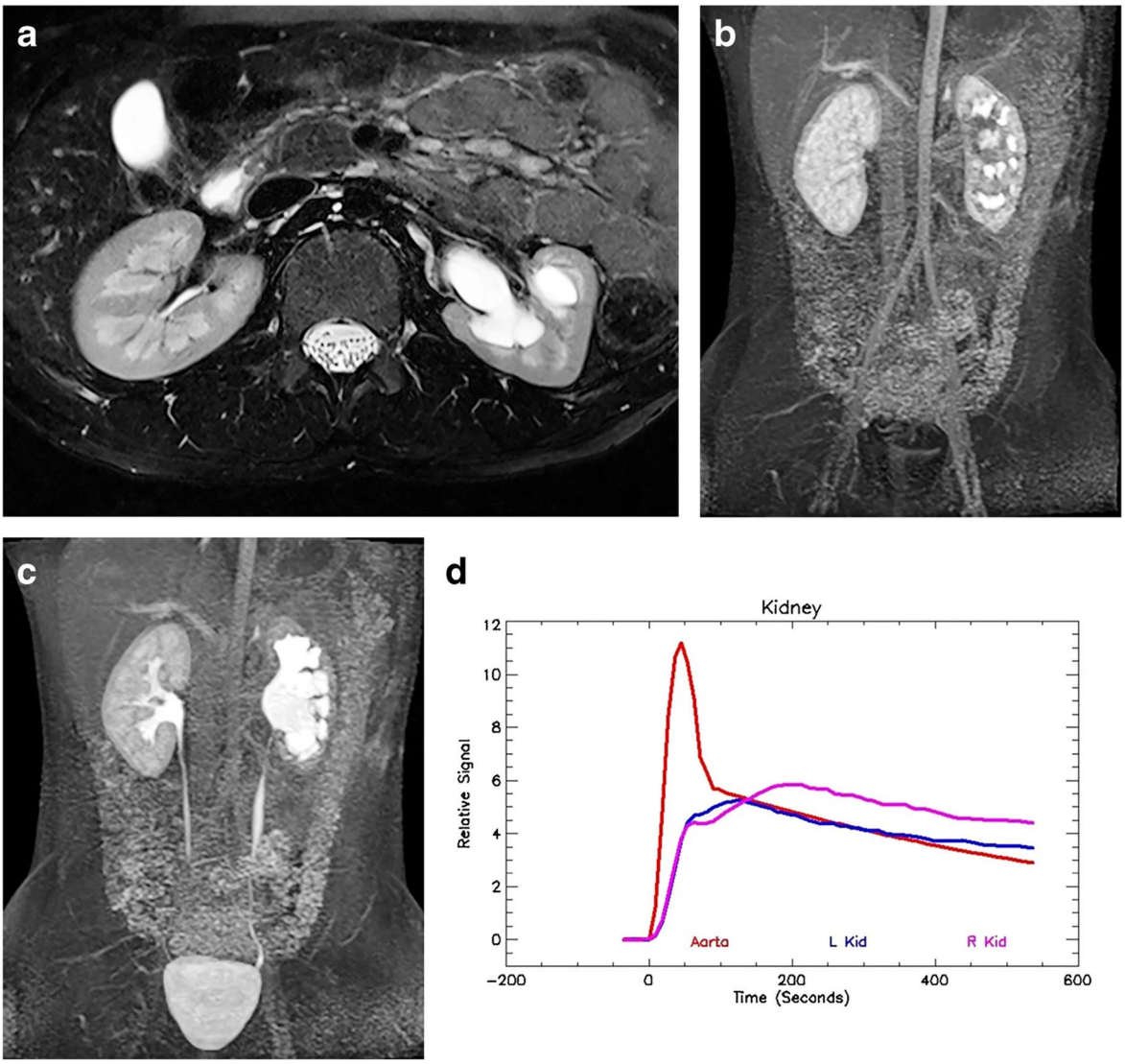

Fig. 4.

Imaging in a 9-year-old boy (same as in Fig. 3) following successful pyeloplasty. **a** Axial T2-weighted MR image shows significant improvement in the left-side hydronephrosis. The left kidney volume is diminished when compared to the normal right kidney, with significant loss of the renal medulla. **b** Coronal post-contrast maximum-intensity projection (MIP) in the nephrographic phase of the right kidney. Contrast is excreted into the calyces on the left, dramatically changed from the preoperative study. This indicates that the physiologically significant obstruction has been relieved by the pyeloplasty and that rapid calyceal excretion is largely related to a left-side concentration defect secondary to the medullary volume loss. **c** Coronal delayed MIP image shows contrast agent in both ureters, with a decrease in left-side hydronephrosis. Mild persistent narrowing is noted at the left ureteropelvic junction (UPJ), a not uncommon finding following pyeloplasty. **d** Signal intensity versus time curves again show normal aortic and right kidney curves. The left kidney curve has improved with a small concentration peak and improved washout from the renal parenchyma, with the signal paralleling the aortic curve in the later phases. The concentration peak occurred slightly

earlier than in the normal right kidney, which was thought to be related to mild glomerular hyperfiltration. The renal functional analysis was: vDRF L:R = 28:72; pDRF L:R = 33:67; unit Patlak L:R = 0.33:0.26 mL/min/cm^3; asymmetry index = 0.12; MTT, L=35 s, R=62 s. *L* left, *MTT* mean transit time, *pDRF* Patlak differential renal function, *R* right, *vDRF* volumetric differential renal function

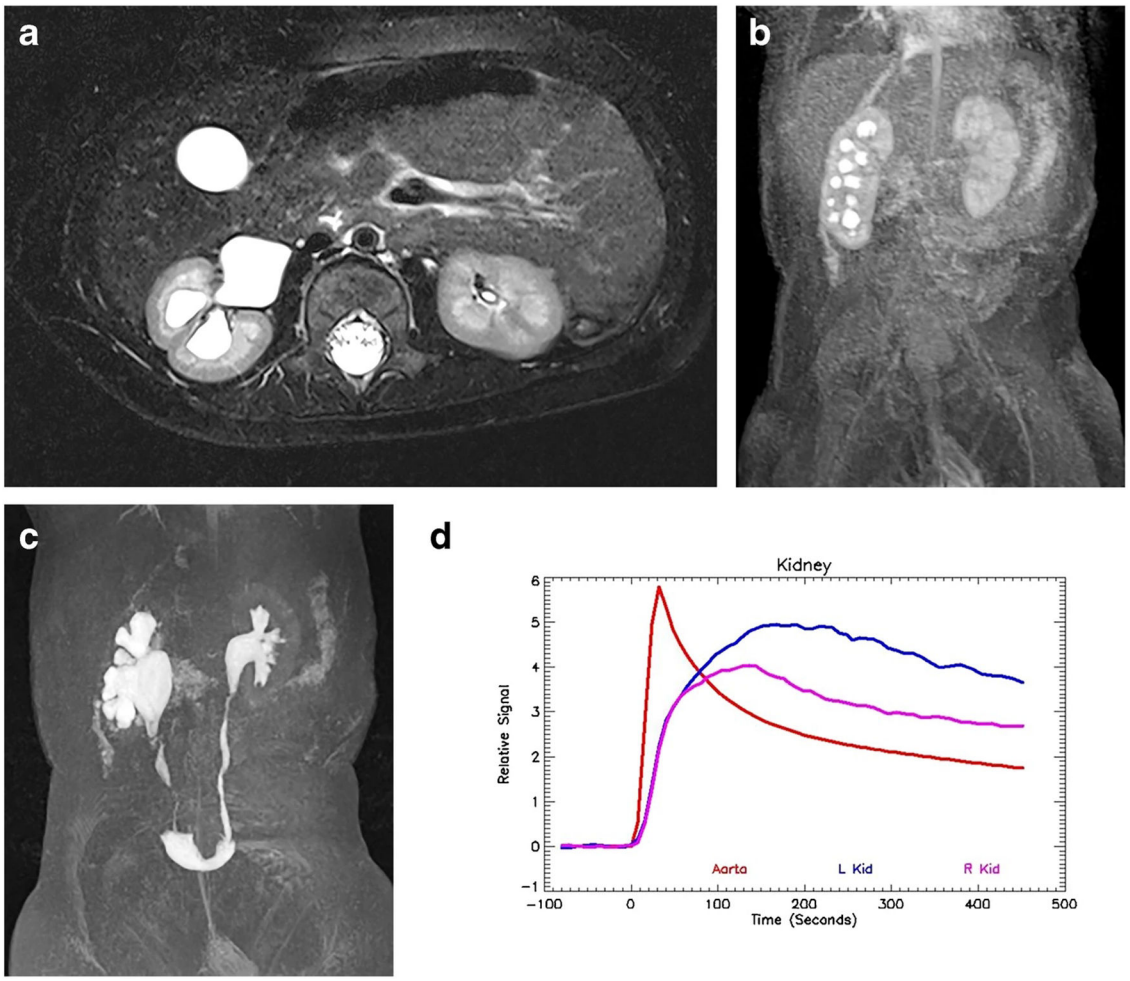

Fig. 5.

Right-side hydronephrosis but no evidence of obstruction in a 6-month-old boy. **a** Axial T2-weighted MR image shows moderate hydronephrosis on the right with mild loss of renal medulla. The left kidney is normal. **b** Coronal post-contrast maximum-intensity projection (MIP) image in the nephrographic phase of the left kidney. Contrast agent is identified in the right-side collecting system, demonstrating rapid calyceal transit time and indicating a compensated hydronephrosis. **c** Coronal delayed MIP image shows contrast agent filling the renal pelvis and ureters bilaterally without evidence of obstruction. **d** Signal intensity versus time curves show that the initial perfusion and early enhancement of the kidneys is symmetrical. However, the right kidney does not concentrate to the same degree as the left, with lower peak amplitude. There is early washout of contrast agent from the renal parenchyma, indicating an underlying tubular concentration defect and no evidence of obstruction. Correlation with the anatomical images is fundamental to interpreting the functional data. The renal functional analysis was: vDRF L:R = 56:44; pDRF L:R = 54:46; unit Patlak L:R = 0.38:0.40 mL/min/cm^3; asymmetry index = 0.04; MTT, L=56 s, R=47 s. *L* left, *MTT* mean transit time, *pDRF* Patlak differential renal function, *R* right, *vDRF* volumetric differential renal function

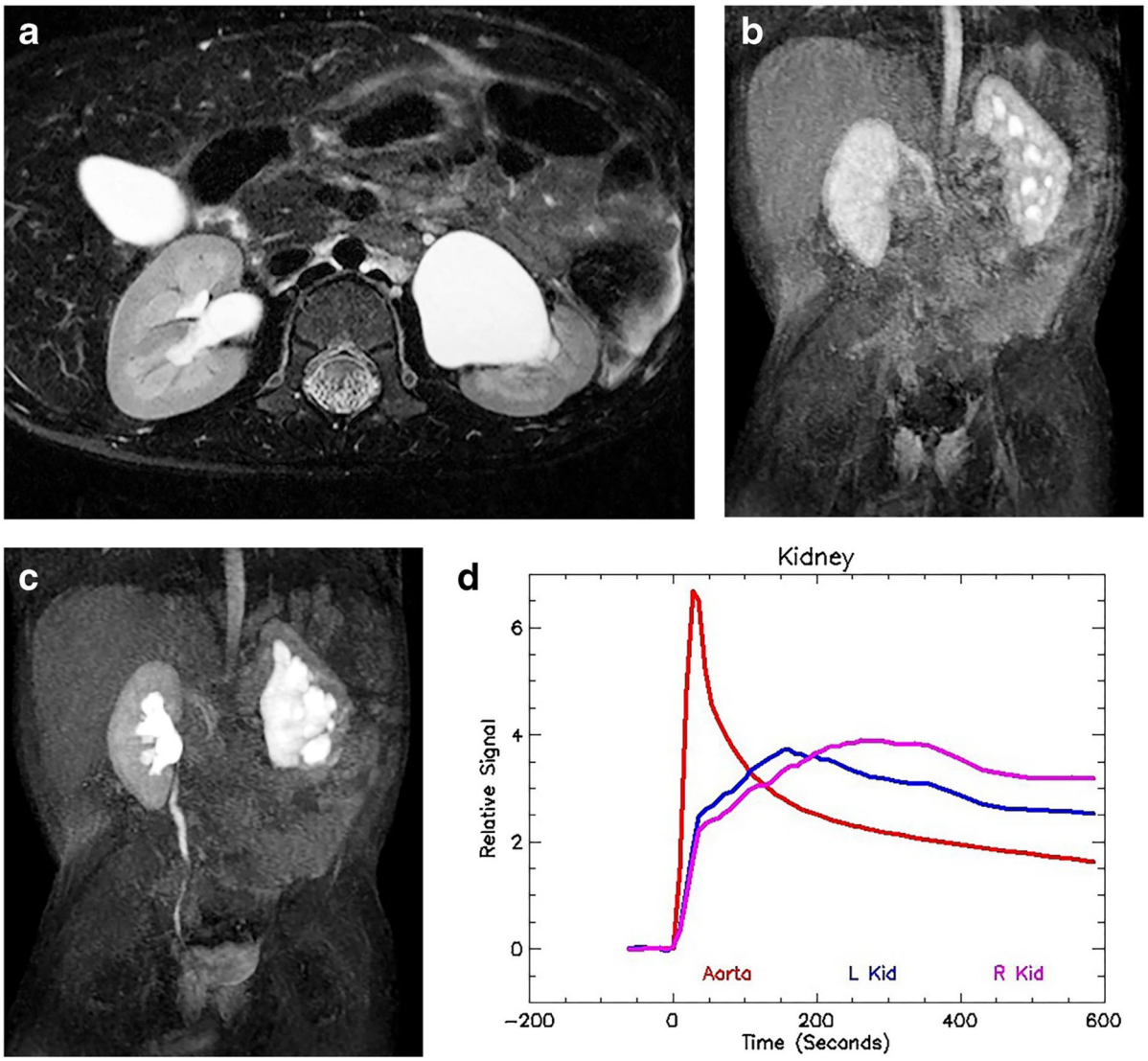

Fig. 6.

Left-side hydronephrosis and glomerular hyperfiltration in a 2-year-old boy. **a** Axial T2-weighted MR image shows moderate hydronephrosis on the left with mild loss of renal medulla. The right kidney is normal. **b** Coronal post-contrast maximum-intensity projection (MIP) image in the nephrographic phase of the right kidney. Contrast agent is identified in the left-side collecting system, demonstrating rapid calyceal transit time. **c** Coronal delayed MIP image shows contrast agent filling the renal pelvis bilaterally, with contrast in the right ureter. The left ureter is not seen, indicating that the renal transit time is delayed on the left as a result of stasis. The rapid calyceal excretion excludes physiologically significant obstruction. **d** Signal intensity versus time curves again show normal aortic and right kidney curves. The left kidney curve has a more rapid upslope with earlier peak concentration and normal washout. The whole curve for the left kidney has been shifted toward the left, indicating glomerular hyperfiltration. Glomerular hyperfiltration has been seen in cases of intermittent ureteropelvic junction (UPJ) obstruction. Without correlation with the anatomical images, it would be difficult to identify the abnormal kidney, let alone

interpret the functional data. The renal functional analysis was: vDRF L:R = 47:53; pDRF L:R = 51:49; unit Patlak L:R = 0.55:0.47 mL/min/cm^3; asymmetry index = 0.08; MTT, L=35 s, R=62 s. *L* left, *MTT* mean transit time, *pDRF* Patlak differential renal function, *R* right, *vDRF* volumetric differential renal function

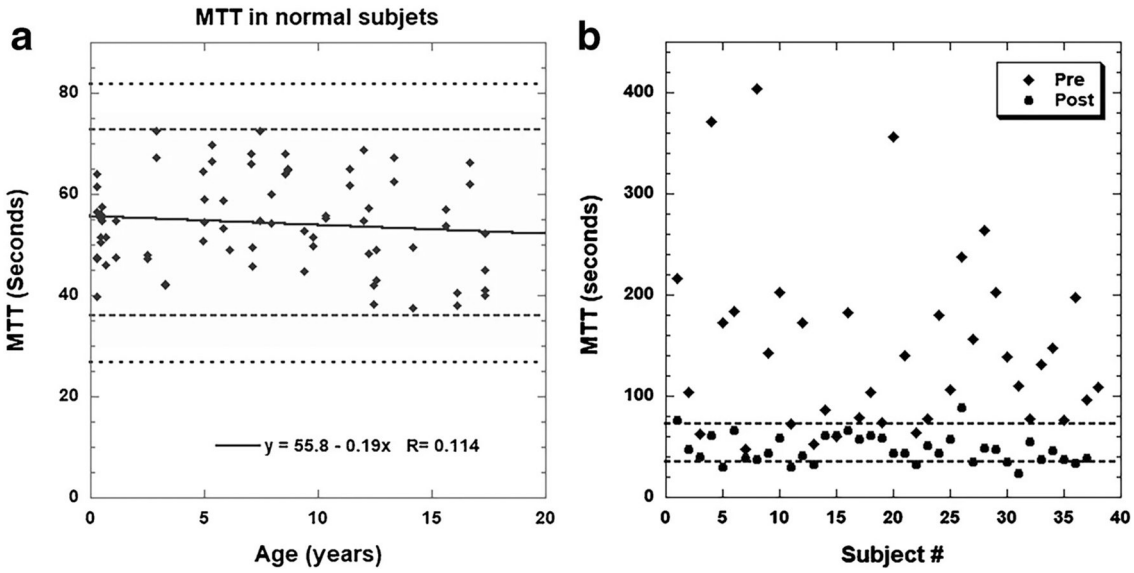

Fig. 7.

Mean transit time (MTT). **a** Using the two-compartment Annet model, we evaluated tubular function by calculating the MTT. In an unpublished study of 38 children with normal-appearing kidneys on MR urography (i.e. 76 kidneys), the MTT was 53.9 s with a standard deviation of 9.4 s. **b** The MTT is another potentially reversible parameter when evaluating hydronephrosis and obstruction. In a group of 37 people with unilateral decompensated ureteropelvic junction (UPJ) obstruction, the average preoperative MTT for the hydronephrotic kidney was 149 s with a standard deviation of 88 s. Following successful pyeloplasty, the average MTT fell to (mean ± standard deviation) 47.8±14 s (J. D. Grattan-Smith, unpublished data). The MTT for the normal contralateral kidneys were 48±14 s preoperatively and 59±9 s postoperatively

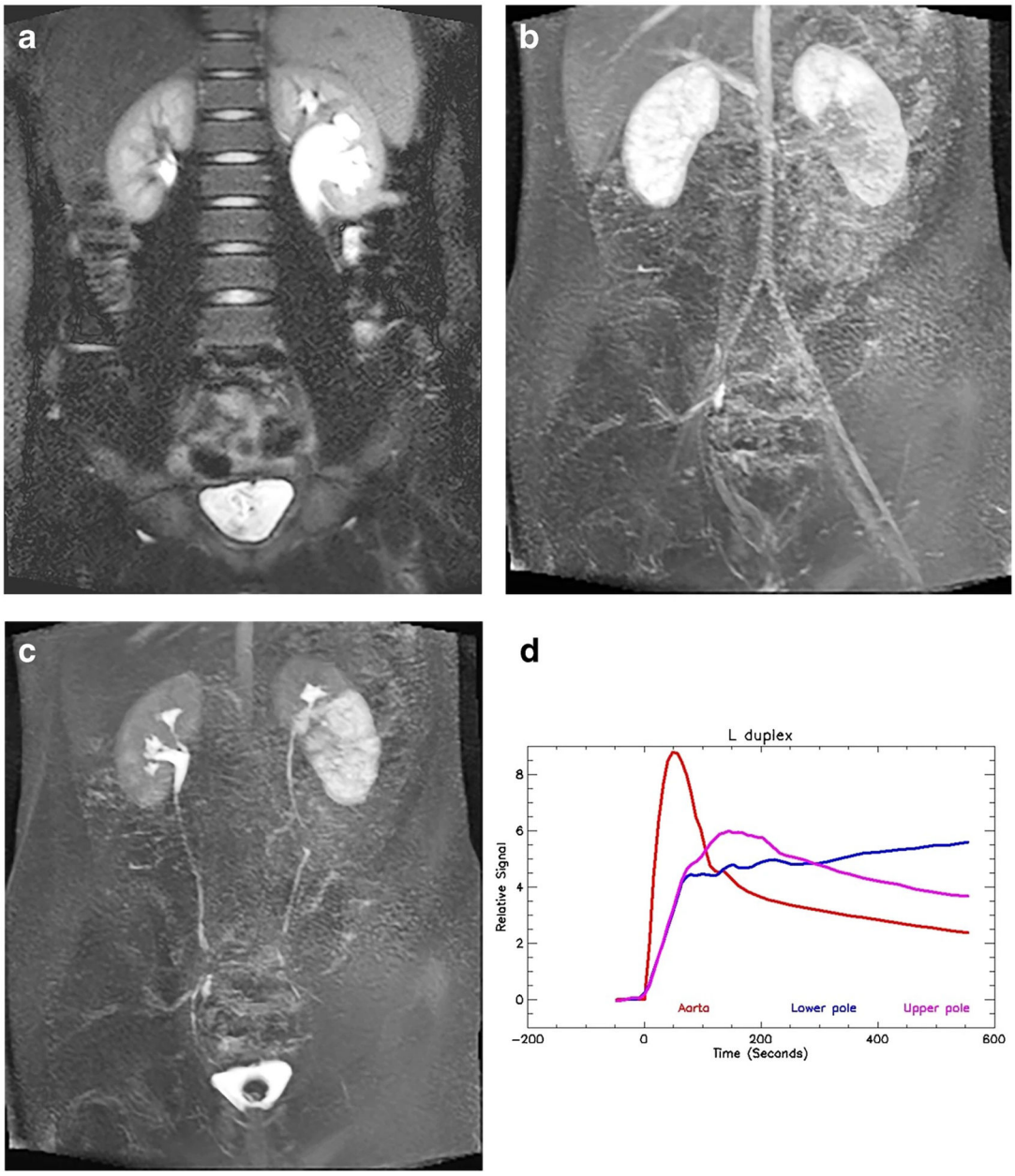

Fig. 8.

Duplex left collecting system and obstructed lower pole moiety in an 11-year-old boy. **a** Coronal T2-W half-Fourier acquisition single-shot turbo spin-echo (HASTE) MR image shows the duplicated left collecting system with a morphological lower-pole ureteropelvic junction (UPJ) obstruction. **b** Coronal post-contrast maximum-intensity projection (MIP) image from the nephrographic phase of the right kidney shows the left upper pole with a similar nephrographic appearance to (**a**), but the lower pole demonstrates delayed enhancement. **c** Coronal post-contrast T1-weighted MIP image shows normal excretion from the right kidney and the left upper pole moiety. The left lower pole moiety demonstrates a delayed and dense nephrogram with delayed calyceal transit time, indicating a physiologically significant obstruction. **d** Signal intensity versus time curves for the left

upper- and lower-pole moieties. The upper pole curve has a normal morphology with normal parenchymal washout. The lower pole moiety shows the delayed and increasingly dense nephrogram, indicating a decompensated UPJ obstruction. The renal functional analysis was: vDRF lower:upper pole = 44:56; pDRF L:R = 36:64; unit Patlak L:R = 0.29:0.51 mL/min/cm^3; asymmetry index = 0.27; MTT, upper pole = 62 s; lower pole = 142 s. *L* left, *MTT* mean transit time, *pDRF* Patlak differential renal function, *R* right, *vDRF* volumetric differential renal function

Table 1

Basic magnetic resonance (MR) urography protocol[a]

Localizer
HASTE sagittal
HASTE coronal
T2 TSE axial kidneys (use radial sequence in older children)
T1 IR coronal (use radial version in older kids)
3-D T2 triggered coronal
2-D TSE axial (bladder)
3-D dynamic coronal (faster is better, use golden angle sequence in older children if available)
POST
Young children
3-D GRE sagittal (~isotropic resolution)
3-D GRE coronal (~isotropic resolution)
Older sedated/non-cooperative children
3-D axial radial sequence (2 stations)
Older non-sedated/cooperative children
3-D GRE breath-hold sagittal
3-D GRE breath-hold coronal
All subjects
2-D axial HASTE (kidneys)

GRE gradient recalled echo, *HASTE* half-Fourier acquisition turbo spin echo, *IR* inversionrecovery, *TSE* turbo spin echo.

[a]Intravenous (IV) furosemide is given approximately 20 min before gadolinium-based contrast agent. Power injection rate depends on IV size, patient size and temporal resolution of dynamic series. The dynamic series should run for at least 5 min and preferably 8 min

Table 2

Definition of parameters used to assess renal function

Calyceal transit time (CTT)	The time required for contrast to pass from the renal cortex in the arterial phase to the dependent portions of the calyces on the maximum-intensity projection (MIP) images of the dynamic, contrast enhanced, sequence.
Renal transit time (RTT)	The time required for the contrast agent to pass from the renal cortex in the arterial phase until it is visualized in the ureter below the lower pole of the kidney on the MIP images of the dynamic post-contrast sequences
Mean transit time (MTT)	The time calculated using a tracer kinetic model with two (or more) compartments and corresponds to the average time for the contrast to pass from the glomerulus into the collecting ducts
Volumetric differential function (vDRF)	The relative volume of enhancing (functional) renal parenchyma of each kidney immediately before contrast is excreted into collecting system relative to the total volume of enhancing parenchyma
Patlak slope (number)	Is calculated using a tracer kinetic model with two (or more) compartments and corresponds to rate at which contrast is filtered at the glomerulus and is related to the individual kidney glomerular filtration rate (GFR)
Patlak DRF	The Patlak number of each kidney relative to the sum of both Patlak numbers
Unit Patlak	Is calculated by dividing the Patlak number for each kidney by the functioning renal volume of that kidney
Asymmetry index	Used to compare the unit Patlak values for each kidney and is an indicator of the degree of functional derangement between the two kidneys irrespective of size

Table 3

Summary of physiological parameters

Physiological state	CTT	RTT	MTT	vDRF	pDRF	Unit Patlak
Decompensated	Delayed	Delayed	Prolonged	Stable	Decreased	Decreased
Compensated	Symmetrical/rapid	Variable	Symmetrical/rapid	Stable	Symmetrical with vDRF	Symmetrical
Hyperfiltration	Rapid	Variable	Rapid	Stable	Increased	Increased
Concentration defect	Rapid	Variable	Rapid	Stable	Symmetrical	Symmetrical

CTT calyceal transit time, *MTT* mean transit time, *pDRF* Patlak differential renal function, *RTT* renal transit time, *vDRF* volumetric differential renal function